On the Performance of Spin Diffusion NMR Techniques in Oriented Solids: Prospects for Resonance Assignments and Distance Measurements from Separated Local Field Experiments

Nathaniel J. Traaseth,[†] T. Gopinath,[†] and Gianluigi Veglia*[,†,‡]

Department of Chemistry, University of Minnesota, Minneapolis, Minnesota 55455, and Department of Biochemistry, Molecular Biology, and Biophysics, University of Minnesota, Minneapolis, Minnesota 55455

Received: June 21, 2010; Revised Manuscript Received: August 31, 2010

NMR spin diffusion experiments have the potential to provide both resonance assignment and internuclear distances for protein structure determination in oriented solid-state NMR. In this paper, we compared the efficiencies of three spin diffusion experiments: proton-driven spin diffusion (PDSD), cross-relaxation-driven spin diffusion (CRDSD), and proton-mediated proton transfer (PMPT). As model systems for oriented proteins, we used single crystals of *N*-acetyl-L-^{15}N-leucine (NAL) and *N*-acetyl-L-^{15}N-valyl-L-^{15}N-leucine (NAVL) to probe long and short distances, respectively. We demonstrate that, for short ^{15}N/^{15}N distances such as those found in NAVL (3.3 Å), the PDSD mechanism gives the most intense cross-peaks, while, for longer distances (>6.5 Å), the CRDSD and PMPT experiments are more efficient. The PDSD was highly inefficient for transferring magnetization across distances greater than 6.5 Å (NAL crystal sample), due to small ^{15}N/^{15}N dipolar couplings (<4.5 Hz). Interestingly, the mismatched Hartmann−Hahn condition present in the PMPT experiment gave more intense cross-peaks for lower ^{1}H and ^{15}N RF spinlock amplitudes (32 and 17 kHz, respectively) rather than higher values (55 and 50 kHz), suggesting a more complex magnetization transfer mechanism. Numerical simulations are in good agreement with the experimental findings, suggesting a combined PMPT and CRDSD effect. We conclude that, in order to assign SLF spectra and measure short- and long-range distances, the combined use of homonuclear correlation spectra, such as the ones surveyed in this work, are necessary.

Introduction

Oriented solid-state NMR is an important technique that allows anisotropic NMR parameters such as chemical shift (CS) and dipolar coupling (DC) to be measured directly.[1] Using this approach, it is possible to resolve the orientation and structure of liquid crystalline molecules and the structure and topology of membrane proteins within lipid bilayers.[1−11] To accurately probe membrane protein topology, separated local field (SLF) experiments such as PISEMA,[12,13] SAMPI4,[14] HIMSELF,[15] and their sensitivity-enhanced variants[16−18] are used to measure DC and CS. These observables are then incorporated into structural refinement protocols essentially as dihedral angle restraints.[7,19−21]

For membrane proteins, SLF-type spectra are assigned using selectively and/or uniformly labeled samples that rely on the periodic nature of the DC and CS (polar index slant angle, PISA, wheel pattern[22,23]) that results from the periodicity of secondary structures (helices and sheets) commonly present in membrane proteins.[24,25] While it has been useful in assigning resonances for structural restraints, this approach heavily relies on the assumption of helix ideality (e.g., ideal dihedral angles for α-helices) as well as the use of several selectively labeled samples. Although membrane helix ideality has been shown to constitute a good approximation,[26] deviations can lead to incorrect assignments and a general bias toward ideal structures. Therefore, sequential assignment strategies such as those employed in solution NMR or magic angle spinning (MAS) techniques are preferred.[27−29,58] Unfortunately, membrane protein dynamics and mosaic spread[30] in mechanically aligned lipid bilayer samples result in severe inhomogenous line broadening (10−15 ppm in ^{15}N linewidths).[31,32] The implementation of magnetically aligned lipid bicelles have overcome many of the limitations in glass plate samples such as maintaining a constant level of hydration,[2,5,33,34] which has substantially decreased mosaic spread and led to increases in signal-to-noise and sample reproducibility.

There are three homonuclear correlation experiments currently used in oriented solid-state NMR: proton-driven spin diffusion (PDSD),[35,36] cross-relaxation-driven spin diffusion (CRDSD),[37] and proton-mediated proton transfer (PMPT)[38] (Figure 1). The preparation periods (90° and cross-polarization) and t_1 chemical shift evolution of these pulse sequences are identical (Figure 1), with the only differences occurring in the mixing elements used for spin diffusion. The PDSD contains a mixing element with no radio-frequency (RF) spinlocks applied to either nucleus. This experiment has had limited application to membrane proteins mechanically aligned on glass plates,[39,40] and is widely believed to be too inefficient for resonance assignment. For these reasons, two exchange sequences, CRDSD[37] and PMPT[38] (similar to PAR experiments in MAS[41−43]), were developed. The mixing period for the CRDSD experiment utilizes a weak RF spinlock amplitude on ^{15}N to *drive* the spin diffusion among the ^{15}N nuclei, while the PMPT sequence, in addition to the *Z*-filter, contains a cross-polarization element mismatched with respect to the Hartmann−Hahn condition. The PMPT experi-

* Corresponding author. Address: 6-155 Jackson Hall 321 Church St SE Minneapolis, MN 55455. Phone: (612) 625 0758. E-mail: vegli001@umn.edu.
[†] Department of Biochemistry, Molecular Biology, and Biophysics.
[‡] Department of Chemistry.

10.1021/jp105718r
Published on Web 10/11/2010

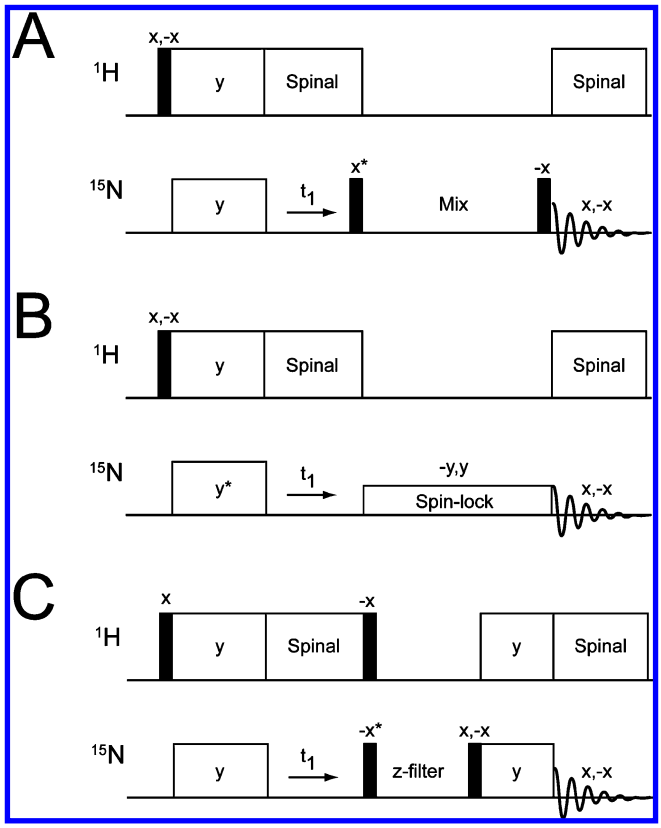

Figure 1. Pulse sequences used to obtain homonuclear $^{15}N/^{15}N$ correlation spectra: (A) proton-driven spin diffusion (PDSD), (B) cross-relaxation-driven spin diffusion (CRDSD), and (C) proton-mediated proton transfer (PMPT). Asterisks indicate pulses that were adjusted by a 90° phase-shift to acquire phase-sensitive data in the indirect dimension.

ment was recently shown to be useful in assigning SLF spectra for Pf1 phage coat protein.[44]

In oriented solid-state NMR, there has not been a parallel comparison of the three spin diffusion methods on the same system. The CRDSD experiment was tested with a single crystal of the dipeptide N-acetyl-L-^{15}N-valyl-L-^{15}N-leucine (NAVL), while PMPT was originally evaluated using a crystal of N-acetyl-L-^{15}N-leucine (NAL). These crystals differ in the nearest interatomic distances between ^{15}N spins: 3.3 and 6.5 Å for NAVL and NAL, respectively. In this study, we systematically assessed the efficiency of PDSD, CRDSD, and PMPT with both NAL and NAVL crystals. We found that the PDSD is the most efficient for short distances and for assignment, while CRDSD and PMPT are more suitable for longer distance correlations.

Experimental Methods

NMR Spectroscopy. ^{15}N labeled single crystals of NAL and NAVL were prepared as previously described.[45] NMR experiments were conducted on a VNMRS Varian system operating at a ^{1}H Larmor frequency of 700 MHz. The two crystals were placed in arbitrary orientations with respect to the magnetic field in order to maximize the dispersion of ^{15}N resonances. All spin diffusion experiments were conducted on the same crystal orientations using a double resonance low-E probe.[46] For all experiments, including the PISEMA, PDSD, CRDSD, and PMPT (see Figure 1), 4 or 16 scans (NAL or NAVL, respectively) were acquired for each t_1 increment with a 3 s recycle delay between scans. The spectral widths for the homonuclear $^{15}N/^{15}N$ spectra were 10 and 50 kHz for the indirect and direct dimensions with total acquisition times of 4 and 10 ms, respectively. For the PDSD experiments, we employed mixing periods from 1 to 30 s for NAL and from 1 to 20 s for NAVL. The ^{15}N radio-frequency-driven spin diffusion (RFDSD)[47,48] experiments were conducted by varying the ^{15}N RF amplitude ($\omega_S/2\pi$, also called the mean ^{15}N Rabi frequency) from 0 to 50 kHz with no proton spinlock. The CRDSD experiments[37] were performed by adjusting the mixing time from 1 to 20 ms using a ^{15}N spinlock of 21 kHz (optimized value from RFDSD). For the PMPT experiments,[38] three variables were adjusted. First, spectra were acquired by varying the ^{1}H RF amplitude ($\omega_I/2\pi$, also called the mean ^{1}H Rabi frequency) during mismatch-Hartmann−Hahn (mmHH) from 0 to 70 kHz at three ^{15}N RF spinlock amplitudes ($\omega_S/2\pi$ = 21, 37.5, and 52.5 kHz) at a mixing time of 10 ms. The ^{1}H RF amplitudes that gave the most intense cross-peaks were used to perform mixing time buildup curves from 1 to 20 ms. All 2D experiments were then acquired in a pseudo-3D interleaved fashion to minimize experimental errors.

Numerical Simulations. PMPT and CRDSD experiments were simulated by considering 12 spins (two ^{15}N nuclei, spin S, and 10 ^{1}H nuclei, spin I). The rotating frame Hamiltonian in the presence of on-resonance RF pulses on I and S spins is given by

$$H = \omega_S(S_{1x} + S_{2x}) + \omega_I \sum_{i=1}^{N} I_{ix} + H_{IS} + H_{II} + H_{SS}$$

$$H_{IS} = \sum_{i=1}^{N} [d_{1i} S_{1z} I_{iz} + d_{2i} S_{2z} I_{iz}]$$

$$H_{II} = \sum_{i<j}^{N} b_{ij} [I_{iz} I_{jz} - \frac{1}{4}(I_{+i} I_{-j} + I_{-i} I_{+j})]$$

$$H_{SS} = b_{12}\left[S_{1z} S_{2z} - \frac{1}{4}(S_{+1} S_{-2} + S_{-1} S_{+2})\right] \quad (1)$$

H_{IS} is the heteronuclear dipolar Hamiltonian, H_{II} and H_{SS} are the homonuclear dipolar Hamiltonians, ω_I and ω_S are RF amplitudes for spins I and S, S_+ and I_+ are raising operators, S_- and I_- are lowering operators, S_{ix}, S_{iz}, I_{ix}, and I_{iz} are Cartesian operators, and d_{ij} and b_{ij} are the hetero- and homonuclear dipolar couplings between nuclei i and j, respectively. The simulations were carried out with N = 10. In order to calculate all d_{ij} and b_{ij} values for NAL, we performed a PISEMA experiment to measure CS and DC values for the four unique ^{15}N sites. These observables were then used to rotate the crystal coordinate file of NAL (CCDC 624793) to best match the experimental values. After optimization, two ^{15}N nuclei were chosen that had the closest distances in the crystal (6.5 Å), corresponding to a $^{15}N/^{15}N$ dipolar coupling of 3.2 Hz. In addition, 10 protons were selected that had >30 Hz dipolar couplings with both ^{15}N nuclei. All dipolar couplings used for the simulation are given in Supporting Information Table I. In order to calculate the transfer efficiency between the two ^{15}N spins, $G(t)$, we evaluated the following equation in MATLAB (MathWorks, Natick, MA) for several mixing times (t) ranging from 0 to 40 ms (1 ms intervals):

$$G(t) = \mathrm{Trace}(S_{1x} e^{-iHt} S_{2x} e^{iHt}) \quad (2)$$

PMPT and CRDSD experiments were simulated by varying the ^{1}H RF spinlock amplitude (ω_I) from 0 to 70 kHz (in 2.5 kHz

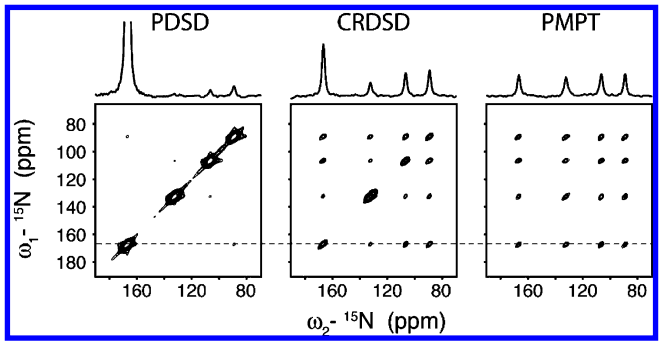

Figure 2. Comparison of spin diffusion experiments on NAL. Note that the peak naming convention (peaks a, b, c, d) is from the most downfield (peak a) to the most upfield (peak d). For example, the cross-peak at $\omega_2 = 167$ ppm and $\omega_1 = 133$ ppm is labeled ab. The PDSD experiment utilized a 3 s mixing time, the CRDSD experiment a ^{15}N RF amplitude of 21 kHz, and the PMPT experiment a *Z*-filter of 3 s and ^{1}H and ^{15}N RF amplitudes of 30 and 21 kHz, respectively. The CRDSD and PMPT experiments used a mixing time of 10 ms. 1D sections are taken from the dotted line in the 2D spectra. All 2D spectra are shown at the same contour level, allowing for a direct comparison of peak intensities.

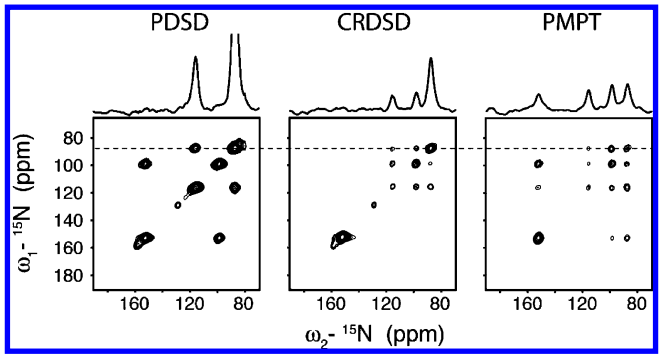

Figure 3. Comparison of spin diffusion experiments on NAVL. Note that the peak naming convention (peaks a, b, c, d) is from the most downfield (peak a) to the most upfield (peak d). For example, the cross-peak at $\omega_2 = 152$ ppm and $\omega_1 = 99$ ppm is labeled ac. The PDSD experiment utilized a 3 s mixing time, the CRDSD experiment a ^{15}N RF amplitude of 21 kHz, and the PMPT experiment a *Z*-filter of 3 s and ^{1}H and ^{15}N RF amplitudes of 65 and 55 kHz, respectively. The CRDSD and PMPT experiments used a mixing time of 10 ms. 1D sections are taken from the dotted line in the 2D spectra. All 2D spectra are shown at the same contour level, allowing for a direct comparison of peak intensities.

intervals) for each of three ^{15}N RF amplitudes ($\omega_S/2\pi = 17.5$, 33, and 50 kHz). Note that, for the simulation of the CRDSD experiment, $\omega_I = 0$. The complete Hamiltonian in eq 1 was used in eq 2, with no motional processes or relaxation accounted for in the simulation.

Results

Spin Diffusion between ^{15}N/^{15}N Nuclei in NAL and NAVL. The single crystals of NAL and NAVL were placed at an arbitrary orientation and kept in this position for all of the measurements. The nearest distances between ^{15}N nuclei in NAVL and NAL are 3.3 and 6.5 Å, which are good mimics of *i*, *i*+1 and *i*, *i*+4 ^{15}N/^{15}N distances in an ideal α-helix (~3 and ~6 Å). Both NAL and NAVL gave four unique ^{15}N resonances, resulting in 12 total cross-peaks in each homonuclear 2D ^{15}N/^{15}N correlation spectrum. Figures 2 (NAL) and 3 (NAVL) show the results from 2D spectra acquired using PDSD, CRDSD, and PMPT experiments. The noise floor in both figures is the same for all three spectra, so the cross-peak intensities for the three pulse sequences can be directly compared. For NAL, the PDSD experiment was found to be the most inefficient, with very weak cross-peaks. In contrast, the CRDSD and PMPT experiments both were quite efficient for long ^{15}N/^{15}N distances found within NAL, resulting in observation of all cross-peaks. This result supports previous experiments in which ^{15}N/^{15}N distances up to 8.5 Å were detected.[38,49] For the NAVL crystal, the PDSD experiment gave significantly more intense cross-peaks than the NAL crystal. In fact, the intensities were larger than those detected using either the CRDSD or PMPT experiment. In the following sections, we compare the three experiments, adjusting systematically the experimental parameters to maximize cross-peak intensities in ^{15}N/^{15}N (or ^{13}C/^{13}C) correlation spectra for both short and long distances (e.g., mixing times and RF amplitudes). All data for NAL and NAVL are shown at the same noise floor for each experiment.

Note that another spin diffusion experiment referred to as CHHC or NHHN has shown to be quite useful in MAS solid-state NMR.[50] While we were able to observe ^{15}N/^{15}N cross-peaks in NAL using NHHN, the signal-to-noise was only a fraction of that observed with PDSD, CRDSD, or PMPT, and we therefore did not further pursue this pulse sequence. Proton−proton mixing has, however, been shown to be useful in some oriented solid-state NMR experiments.[51]

Proton-Driven Spin Diffusion. The dependence of the spin diffusion probability (Ω) on the dipolar coupling strength between two nuclei (ω_{ij}) is given by Fermi's golden rule:[36,52]

$$\Omega = \frac{1}{2}\pi F_{ij}(0)\omega_{ij}^{2}t \qquad (3)$$

$F_{ij}(0)$ is the zero-quantum line shape and t is the time for spin diffusion to take place. Since the dipolar coupling is proportional to r_{ij}^{-3} (r is the distance between nuclei), the probability for a transition between two ^{15}N nuclei is quite small for $r_{ij} > 6.5$ Å and $t < 5$ s (i.e., ^{15}N/^{15}N dipolar couplings < 4.5 Hz). For the NAL crystal, where the nearest ^{15}N/^{15}N distances are 6.5, 6.7, and 8.5 Å, the buildup of magnetization as a function of mixing time is highly inefficient (Figure 4 and Supporting Information Figure 1). At a mixing time of 30 s, the cross-peak displaying the most efficient transfer rate (cross-peak intensity divided by diagonal peak intensity) approaches only 20% (Supporting Information Figure 1), as expected from eq 3.

For the NAVL single crystal, the results (Figure 5 and Supporting Information Figure 2) agree well with the theoretical ω_{ij}^{2} dependence in eq 3, showing an efficient transfer of magnetization for intramolecular ^{15}N sites (a/c and b/d) and a substantially more inefficient transfer for intermolecular ^{15}N nuclei. Due to the shorter intramolecular distance between ^{15}N spins of 3.3 Å (^{15}N/^{15}N dipolar couplings < 35 Hz),[45] the magnetization was almost completely transferred at ~10 s with ~50% efficiency at ~3−4 s (Supporting Information Figure 2). In contrast, at mixing times of 20 s, the transfer efficiency is only 40% between intermolecular sites, indicating that the PDSD has a clear distance dependence. While a mixing time of 5−10 s is somewhat long, the relaxation in the PDSD experiment is dominated by T_1, which is very long for ^{15}N magnetization, leading to strong cross-peaks in NAVL.

Cross-Relaxation-Driven Spin Diffusion. The CRDSD mechanism has been reported to be highly efficient for transferring magnetization in the NAVL crystal.[37] Unlike the PDSD experiment (Figure 1), there are two variables that need to be independently optimized to achieve the most favorable transfer: (1) the ^{15}N RF spinlock amplitude and (2) the mixing time.

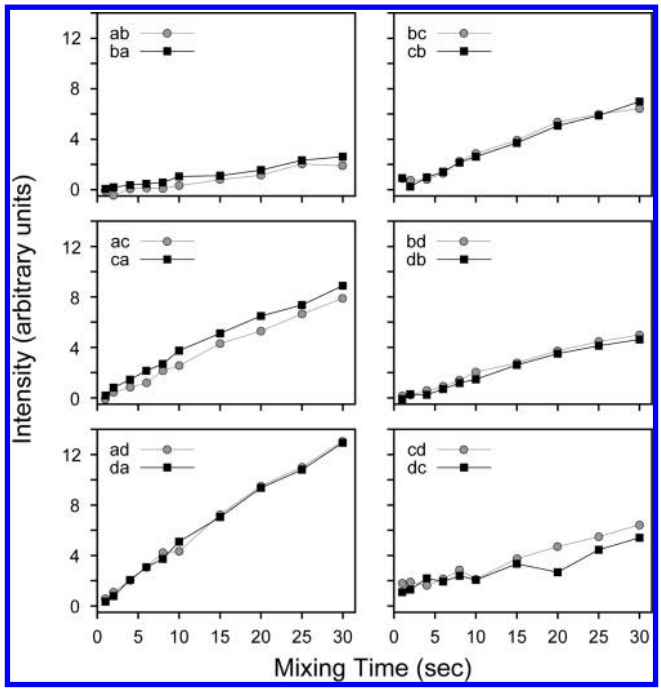

Figure 4. PDSD experiments on the NAL single crystal. All 12 cross-peaks shown from the spectra are shown in arbitrary intensity units. All experiments from the NAL crystal (Figures 6, 8, 10, and 11) are shown in the same relative intensity units (i.e., same noise floor).

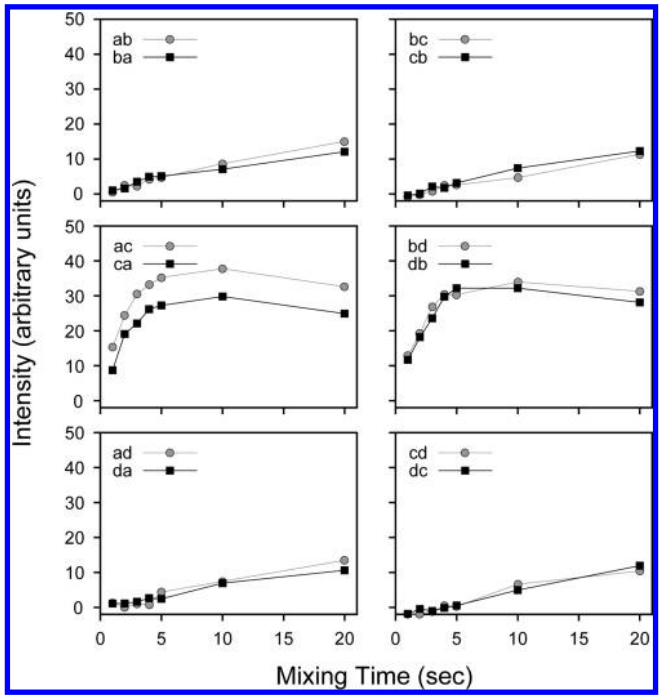

Figure 5. PDSD experiments on the NAVL single crystal. All 12 cross-peaks shown from the spectra are shown in arbitrary intensity units. All experiments from the NAVL crystal (Figures 7, 9, and 12) are shown in the same relative intensity units (i.e., same noise floor).

Figure 6 shows changes in the cross-peak intensities in NAL upon variation of the ^{15}N RF amplitude for a 10 ms mixing time. Due to relaxation during the spinlock (from multiple relaxation channels), we plot the absolute intensity of the cross-peaks rather than the normalized cross-peak intensity to analyze these results.[53,54] The maximum intensity of all cross-peaks occurs for $\omega_s/2\pi = 17-22$ kHz (Figure 6). A similar range was found to give maximal cross-peak heights in the NAVL

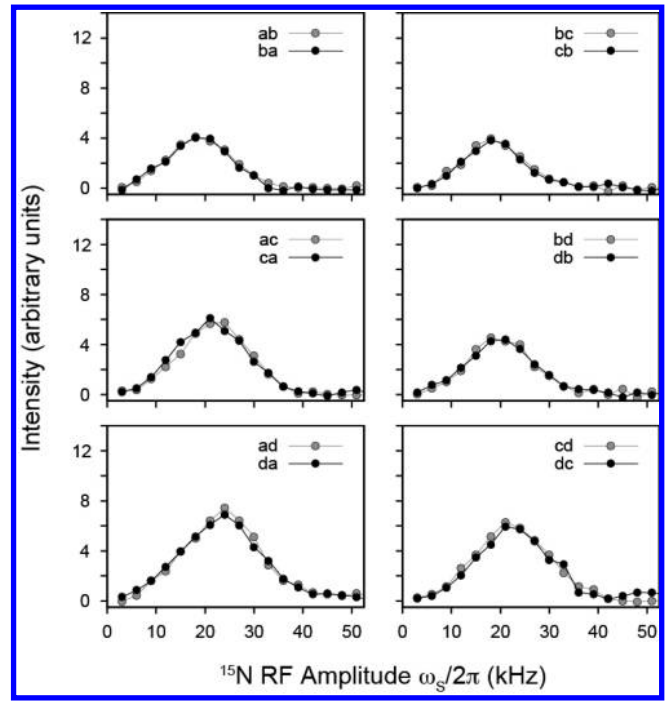

Figure 6. CRDSD experiments on the NAL single crystal. The ^{15}N RF amplitude was varied while keeping the mixing time fixed at 10 ms. The intensities are expressed in arbitrary units. All experiments were acquired in an interleaved manner to avoid potential differences in the experiments, and are therefore relevant to compare within each panel.

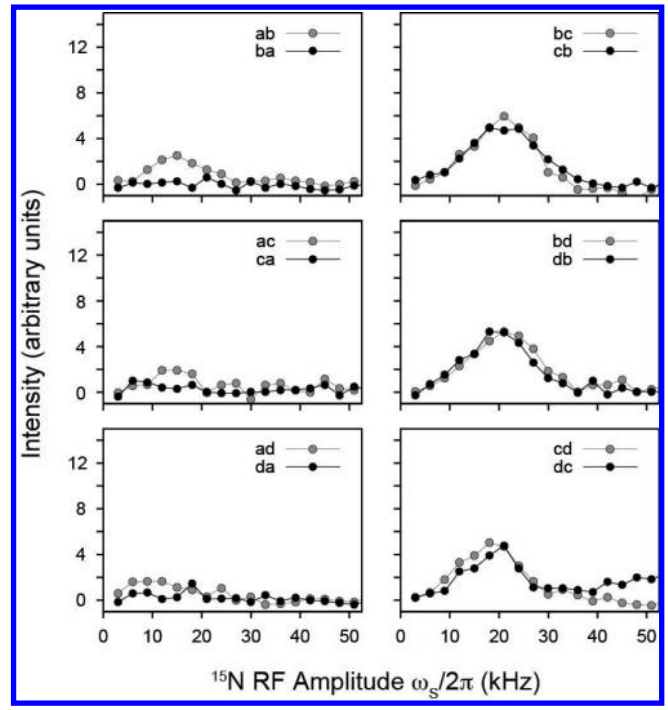

Figure 7. CRDSD experiments on the NAVL single crystal. The ^{15}N RF amplitude was varied while keeping the mixing time fixed at 10 ms. The intensities are expressed in arbitrary units.

dipeptide crystal,[37] which is in quantitative agreement with our measurements (Figure 7).

We also performed a systematic buildup of the NAL and NAVL cross-peaks by varying the mixing time at a fixed ^{15}N RF amplitude of 21 kHz. From the series of these 2D spectra, we found that the magnetization reached a maximum for all NAL cross-peaks between 5 and 15 ms (Figure 8). Therefore,

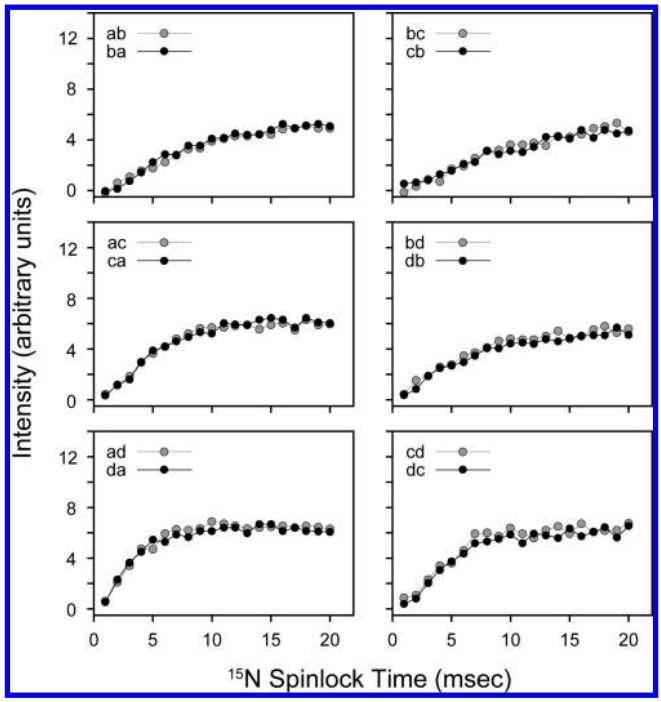

Figure 8. CRDSD experiments on the NAL single crystal. The ^{15}N RF amplitude was fixed at 21 kHz, while the mixing time was varied between 1 and 20 ms. The cross-peak intensities are plotted in arbitrary units.

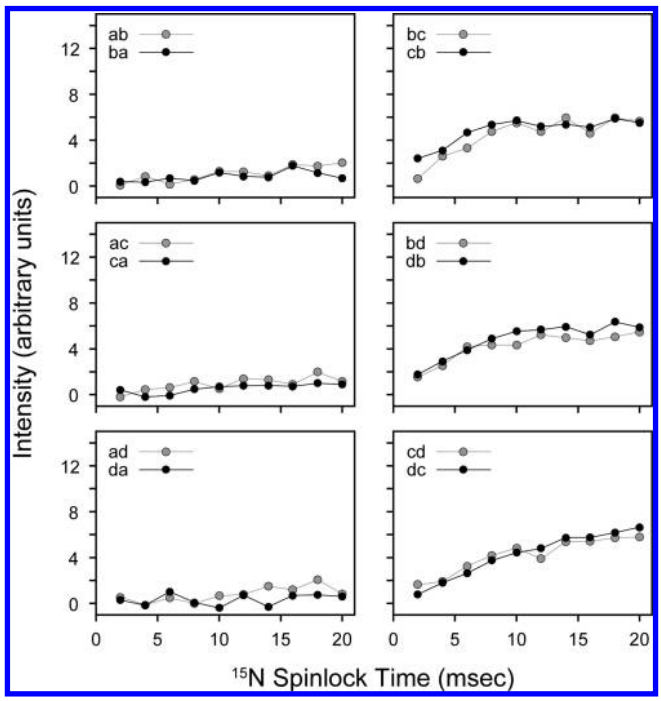

Figure 9. CRDSD experiments on the NAVL single crystal. The ^{15}N RF amplitude was fixed at 21 kHz, while the mixing time was varied between 1 and 20 ms. The cross-peak intensities are plotted in arbitrary units.

the magnetization transfer is much more efficient in the CRDSD than the PDSD experiment. In Figure 9, we plot the cross-peak intensities as a function of the mixing time from the NAVL sample, which are consistent with those previously reported[37] (even the crystal orientation is similar). The results obtained for NAL and NAVL suggest that both intra- and intermolecular magnetization transfers proceed essentially at the same rate (Figures 8 and 9). Since the internuclear ^{15}N distances in the crystals are strikingly different, 3.3 vs 6.5 Å, there is a potential problem for using these experiments to sequentially assign resonances. Ideally, for a *walk* through the backbone ^{15}N residues (i.e., sequential resonance assignment), one would only want to correlate residue i with the adjacent $i \pm 1$. The CRDSD mechanism relies on the presence of direct ^{15}N/^{15}N couplings, but the strongly coupled proton network essentially removes the distance dependence of the cross-peak intensities.

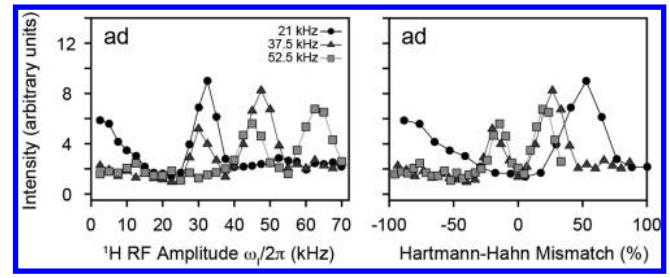

Figure 10. PMPT experiments on the NAL single crystal. The ^{1}H RF amplitude was varied between 0 and 70 kHz for three different ^{15}N RF amplitudes (21, 37.5, and 52.5 kHz). The values are also plotted as the Hartmann−Hahn mismatch percentage. The mixing time was fixed at 10 ms for all points. Cross-peak intensities are plotted in arbitrary units. The dip in the curves is due to the Hartmann−Hahn match. The other cross-peaks are essentially the same as that plotted for the cross-peak ad. All other curves are shown in Supporting Information Figures 3 and 4.

Proton-Mediated Proton Transfer Mechanism. Unlike the PDSD and CRDSD pulse schemes, there are three experimental parameters that need to be optimized for the PMPT experiment: (1) the ^{15}N spinlock, (2) the ^{1}H spinlock (mismatch condition), and (3) the mixing time. It is noted that the PMPT experiment is essentially the oriented solid-state NMR version of the proton assisted recoupling (PAR) experiment used in MAS experiments.[41−43]

To test the PMPT experiment, we first set the mixing time to 10 ms, and then adjusted the ^{1}H RF amplitude at three different ^{15}N spinlocks ($\omega_s/2\pi$ = 21, 37.5, and 52.5 kHz). The PMPT mechanism has previously been reported to be most efficient in NAL when the ^{1}H RF amplitude is mismatched by 110% from that of the ^{15}N spinlock.[38,49] As the ^{1}H spinlock amplitude approaches the Hartmann−Hahn match,[55] part of the magnetization is transferred back to the protons, depleting the observable ^{15}N magnetization. Therefore, there is a trade-off between the efficiency of the proton-mediated transfer mechanism and the Hartmann−Hahn match. Figure 10 shows the cross-peak intensities of NAL as a function of the ^{1}H RF amplitude. We found that two of the curves (^{15}N RF amplitudes of 37.5 and 52.5 kHz) each have two relative maxima that are located above and below the Hartmann−Hahn match. For the 21 kHz ^{15}N spinlock curve, there is only one maximum, which is present above the Hartmann−Hahn matching condition (32 kHz ^{1}H spinlock or 155% of the ^{15}N spinlock value). Interestingly, we found that the absolute cross-peak intensities were actually higher at a lower ^{15}N spinlock value (and therefore ^{1}H RF amplitude) for a mixing time of 10 ms. To further investigate this, we performed a systematic buildup of the mixing time for the three ^{15}N RF amplitudes and the optimized ^{1}H mismatch values (Figure 10). As with the CRDSD mechanism, all of the cross-peaks reached a maximum intensity at 5−10 ms (see Figure 11). A ^{15}N RF amplitude of 21 kHz gave the most intense cross-peaks (Figure 11). This suggests that the mechanism is a combination of both direct ^{15}N/^{15}N couplings (the CRDSD mechanism) as well as the proton-mediated effect (PMPT mechanism).

Next, we analyzed the cross-peak intensities in NAVL as a function of the ^{1}H spinlock for a ^{15}N RF amplitude of 57.5 kHz.

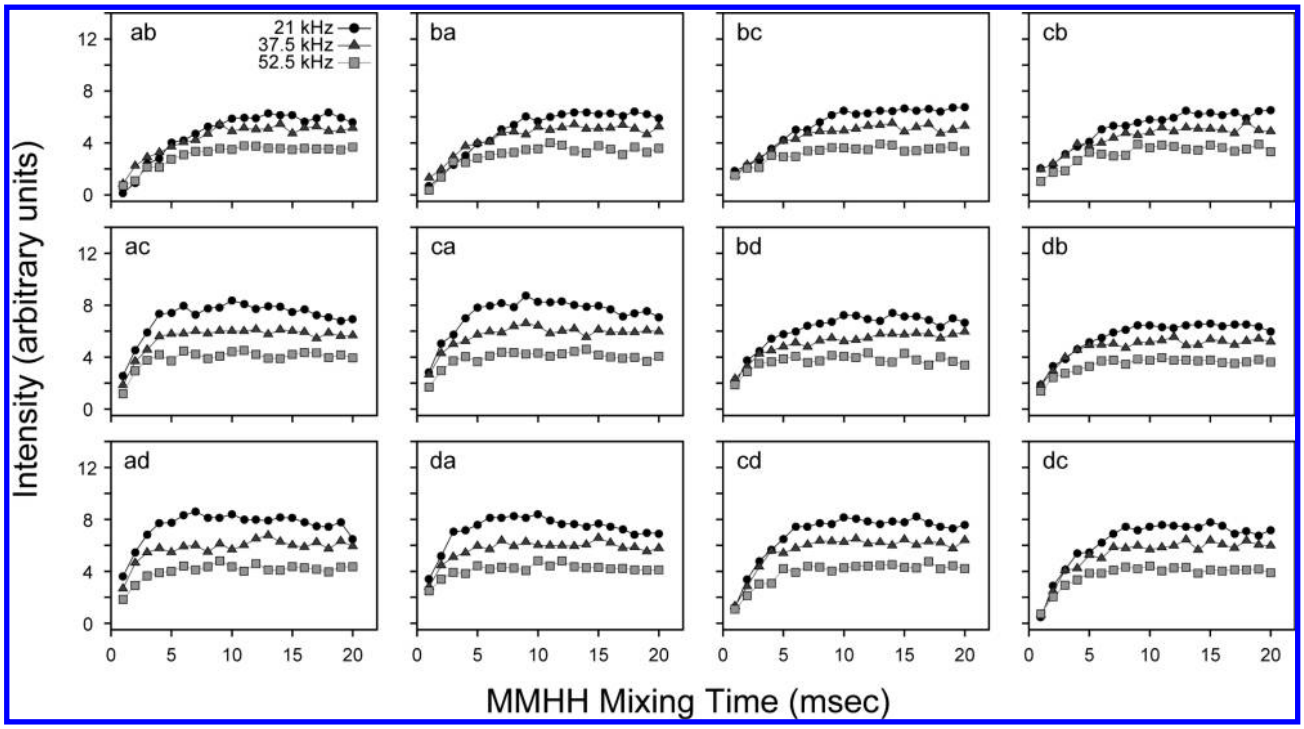

Figure 11. PMPT experiments on the NAL single crystal. The ^{1}H RF amplitudes were set to 32.5, 47.5, and 62.5 kHz for ^{15}N RF amplitudes of 21, 37.5, and 52.5 kHz, respectively, based on the results shown in Figure 10. The mismatched Hartmann−Hahn (MMHH) mixing time was varied from 1 to 20 ms. The cross-peak intensities are in arbitrary units (i.e., not divided by the diagonal peak intensity).

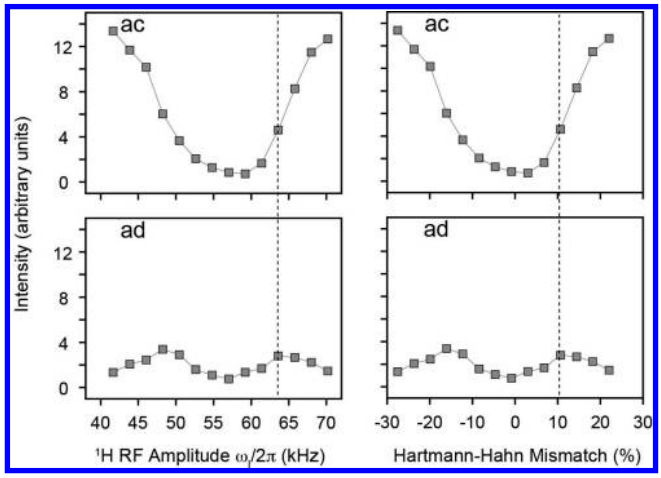

Figure 12. PMPT experiments on the NAVL single crystal. The ^{1}H RF amplitude was varied for a ^{15}N RF amplitude of 57.5 kHz. The mixing time was fixed at 10 ms for all points. The curves plotted are for crosspeaks ac (intramolecular ^{15}N/^{15}N, 3.3 Å) and ad (intermolecular ^{15}N/^{15}N, >6 Å). Intensities are plotted in arbitrary units. The dip in the curves is due to the Hartmann−Hahn match. The dotted line indicates an optimal ^{1}H RF amplitude for intermolecular transfer in NAVL. The optimal value for intermolecular transfer results in less magnetization transfer for intramolecular sites. The other cross-peaks are essentially the same as those plotted for the cross-peaks ac and ad. All other curves are shown in Supporting Information Figures 5 and 6.

The intensity profiles for intermolecular ^{15}N/^{15}N correlations are nearly identical to those found in NAL (compare intermolecular cross-peaks buildup curves for ad in Figures 10 and 12). However, the MMHH condition did not give the maximum intensity for intramolecular peaks (e.g., ac), as indicated by the dotted line in Figure 12. This indicated that the PMPT mechanism only depleted the signal by the transfer of magnetization to ^{1}H (i.e., the Hartmann−Hahn mechanism). In fact, we found that the most efficient transfer for intramolecular ^{15}N nuclei was due to the *Z*-filter element (3 s) used in the pulse sequence (see Figure 1). Indeed, removal of the MMHH element from the PMPT experiment makes the pulse sequence identical to the PDSD experiment, which was shown to give strong intramolecular cross-peaks during the 3 s mixing period for NAVL (Figure 3). These results suggest that PDSD is more efficient for short distances than either PMPT or CRDSD.

Simulations. To validate the results above, we performed numerical simulations of the PMPT and CRDSD experiments for NAL. The DC values used in the simulations were obtained by rotating the NAL crystal coordinates to maximize the agreement with the experimental DCs and CSs measured with a PISEMA experiment. The principal values for the ^{15}N chemical shift tensor were set to $\delta_{11} = 64$, $\delta_{22} = 77$, and $\delta_{33} = 217$ ppm.[56] From this crystal orientation, we calculated all relevant angles relative to the magnetic field, and therefore all dipolar coupling frequencies (b_{ij} and d_{ij} from eq 1; Supporting Information Table I).

The results from the simulation are reported in Figure 13. We set the ^{15}N RF amplitude at values similar to those used in the experiments on NAL (17, 33, and 50 kHz). The ^{1}H spinlock was varied from 0 to 70 kHz, and the time of the transfer, from 0 to 40 ms. In Figure 13A, the transfer efficiencies are plotted as a function of the ^{1}H spinlock at a mixing time of 20 ms. The simulations at three different RF amplitudes clearly show that, at a small ^{15}N RF amplitude, the magnetization transfer is more efficient than those obtained at larger values. Additionally, the CRDSD experiment (^{1}H spinlock = 0 kHz) is reproduced by the simulations: a smaller ^{15}N spinlock of 17.5 kHz gives efficient transfer, while larger ^{15}N RF amplitudes (33, 50 kHz; RFDSD experiment) result in little or no transfer.[37,47] In fact, a low ^{15}N RF amplitude (17 kHz) is unable to completely decouple ^{15}N nuclei from ^{1}H, whereas a larger spinlock amplitude does sufficiently decouple the heteronuclear dipolar coupling.

For the PMPT experiment, the HHMM percentages that give optimal transfer are 29, 21, and 10% for ^{15}N spinlocks of 17.5, 33, and 50 kHz, respectively. This is in agreement with the

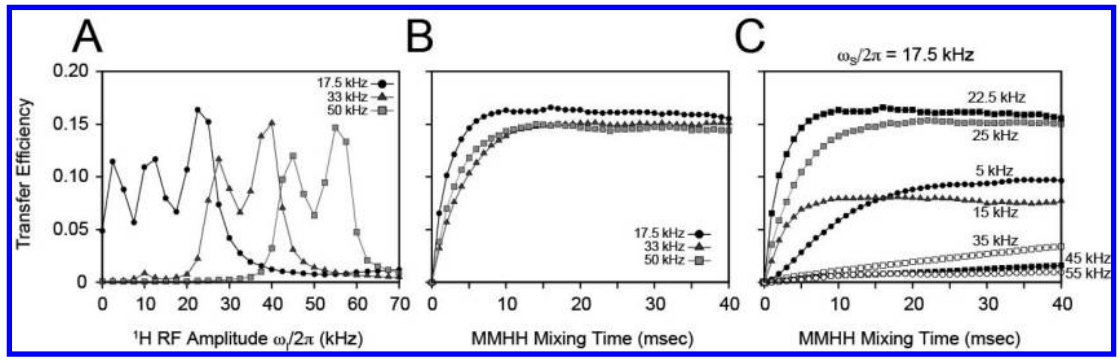

Figure 13. Twelve-spin simulations of the PMPT and CRDSD experiments on the NAL single crystal. (A) The ^{1}H RF amplitude is varied for three different ^{15}N spinlock amplitudes (17.5, 33, and 50 kHz) at a MMHH mixing time of 20 ms. Note that, for a ^{1}H RF amplitude of 0 kHz, this is the CRDSD experiment for a 17.5 kHz ^{15}N spinlock and the RFDSD experiment for larger ^{15}N spinlocks. (B) Buildup for the most optimal transfer efficiencies in panel A. For ^{15}N spinlocks of 17.5, 33, and 50 kHz, the cross-peak intensities were maximal for ^{1}H RF amplitudes of 22.5, 40, and 55 kHz, respectively. (C) Mixing time buildup curves with a ^{15}N spinlock of 17.5 kHz and the ^{1}H RF amplitudes set to the indicated values.

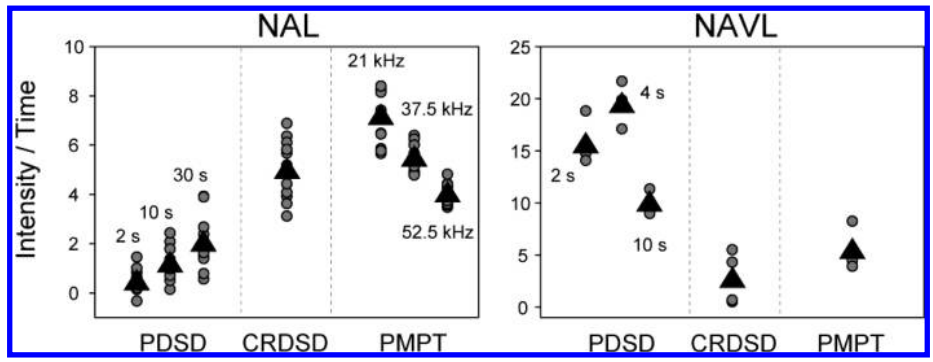

Figure 14. Comparison of PDSD, CRDSD, and PMPT for NAL and NAVL normalized for the mixing time in the PDSD experiment. Since a 3 s recycle delay was used between scans, normalization was done by dividing the PDSD 2D peak intensities by 1.29, 1.53, 2.08, and 3.32 to account for 2, 4, 10, and 30 s mixing times, respectively. No normalization was done for the PMPT experiment, since a shorter *Z*-filter time could have been used that would not have significantly increased the experimental acquisition time.[44] For NAVL, much of the magnetization created in the PMPT experiment originated from the 3 s *Z*-filter time. Circles represent all cross-peaks observed in the NAL spectra and only intramolecular ^{15}N/^{15}N cross-peaks in the NAVL crystal (i.e., peaks ac, ca, bd, and db). Triangles represent the average of the cross-peak intensities shown (values in Table 1). The CRDSD experimental cross-peaks are from the spectra using a 10 ms mixing time with a ^{15}N spinlock of 21 kHz (both NAL and NAVL). The PMPT experimental cross-peaks are from the 10 ms mixing time with the indicated ^{15}N spinlock for NAL and the optimized ^{1}H spinlock used in Figure 11. For NAVL, the PMPT experiment used the 10 ms mixing time with ^{1}H and ^{15}N spinlocks of 65.8 and 57.5 kHz, respectively (same as in Supporting Information Figure 5). It is not appropriate to compare the intensities between NAL and NAVL, as the crystal sizes were different.

experimental values of 55, 27, and 19% obtained for NAL. The deviations from experiment can be accounted for by offset dependencies at lower RF spinlock amplitudes, small errors in the calculation of the experimental spinlock amplitudes, and the approximation of only 12 spins in the simulation. The simulations also show that the transfer efficiencies plotted as a function of the mixing time were in close agreement with those found experimentally. In the simulation, the transfer efficiencies reached a maximum at ~10 ms (Figure 13B), which agrees closely with those reported experimentally in Figures 8 and 11. Taken together, these simulations support the experimental findings that the magnetization in NAL (long distances) is efficiently transferred with both PMPT and CRDSD.

Discussion

In this work, we present a comparison of the spin diffusion experiments currently available for oriented solid-state NMR. While SLF experiments are the most reliable method to directly probe anisotropic structural restraints (DC and CS), no definitive sequential assignment schemes are currently used to accurately and efficiently assign the spectra.

In pursuit of an assignment strategy, we compared the efficiencies of three spin diffusion methods with model compounds that are mimics of short- and long-range distances in proteins (NAVL and NAL). In addition, the ability to detect long-range connectivities for oriented proteins will be useful structural restraints.

In order to compare NAL cross-peak intensities between the PDSD (Figure 4), CRDSD (Figure 8), and PMPT (Figure 11) experiments, we needed to normalize the PDSD data to account for the increased experimental data acquisition time due to the mixing period. The results are plotted in Figure 14 (values in Table 1), and show that the PMPT experiment carried out with low RF amplitudes (^{1}H 32.5 kHz, ^{15}N 21 kHz) gives on average a factor of 3.4 greater intensity per unit time than PDSD (30 s mixing time) and a factor of 1.4 more signal than the CRDSD experiment. Therefore, both the CRDSD and PMPT experiments are highly efficient mechanisms for transferring magnetization at distances up to 8 Å with modest RF amplitudes (17−30 kHz) and mixing times (~10 ms). For the PMPT experiment, we found that the mismatched Hartmann−Hahn condition is most efficient in transferring magnetization at lower RF spinlock amplitudes for ^{1}H and ^{15}N (Figure 14 and Table 1). The latter is an important point, since it is always preferable to use lower powers in experiments to minimize the stress to NMR hardware. While the probes have been improved to handle large RF amplitudes (approaching 100 kHz) for 20 ms under low electric

TABLE 1: The Average Intensity Values per Unit Time for NAL and NAVL as Plotted in Figure 14[a]

NAL	intensity/time	normalized
PDSD (2 s)	0.48	0.067
PDSD (10 s)	1.2	0.17
PDSD (30 s)	2.1	0.29
CRDSD	5.0	0.69
PMPT (21 kHz)	7.2	1.0
PMPT (37.5 kHz)	5.5	0.76
PMPT (52.5 kHz)	4.1	0.57
NAVL	**intensity/time**	**normalized**
PDSD (2 s)	15.7	0.81
PDSD (4 s)	19.5	1.0
PDSD (10 s)	10.1	0.52
CRDSD	2.8	0.14
PMPT	5.5	0.28

[a] The third column shows the data further normalized to 1.0 for the experiment that gave the most intensity/time in NAL and NAVL.

field conditions,[46,57] sample heating still occurs, which is more severe at high magnetic fields.

From the prospective of the sequential resonance assignment in SLF experiments such as PISEMA, HIMSELF, or SAMPI4, the most useful $^{15}N/^{15}N$ correlations are i, $i+1$. This will make the assignments unambiguous and directly amenable to implementing DC and CS restraints in calculating membrane protein structure and topology. A direct comparison of the cross-peak intensities observed for PDSD, CRDSD, and PMPT is shown in Figures 5, 9, and 12, respectively. As for NAL, we calculated the normalized intensity per unit time for NAVL, with the results shown in Figure 14 (values in Table 1). We find that, on average, PDSD with a 4 s mixing time results in the most signal. It gives a factor of 3.5 more signal than the PMPT experiment and a factor of 7 more signal than the CRDSD experiment. Importantly, unlike PDSD, the CRDSD and PMPT sequences essentially erase the distance dependence, making all $^{15}N/^{15}N$ correlations from 3.3 to 8 Å observable with similar cross-peak intensity. In fact, we found that the PMPT experiment with a 3 s *Z*-filter element (acting like a PDSD experiment) significantly reduced cross-peak intensities observed between intramolecular ^{15}N nuclei spaced 3.3 Å apart. Although this might be attractive for long-range distances (e.g., i, $i+4$ distances), it is likely to be problematic for resonance assignments. Recently, a paper by Nevzorov and co-workers introduced the PMPT scheme for assigning membrane proteins. While this method is very promising for measuring long-range distances, the observation of correlations other than i, $i+1$ makes this scheme cumbersome for assignment purposes.[44]

A final consideration is that spinlock experiments such as CRDSD and PMPT result in magnetization that decays with $T_{1\rho}$ (from multiple relaxation channels), whereas the magnetization in the PDSD experiment decays with T_1. Since T_1 in solids is relatively long for ^{15}N spins, the PDSD pulse sequence still might be the most sensitive experiment available for unambiguous resonance assignment of membrane proteins (i.e., correlating only i, $i+1$ resonances). Since its first application in oriented experiments on glass plates, there have been no reported uses of this pulse sequence for assignment purposes, presumably due to the significant inhomogenous line broadening present in the spectra, leading to poor signal-to-noise. Bicelle technology will likely allow these experiments to be usable for sequential assignment (PDSD) and long-range distance restraints (CRDSD and PMPT).[44]

Acknowledgment. This work was supported by the National Institutes of Health (Grants GM64742, HL80081, and GM072701 to G.V.). We thank Professor Alex Nevzorov for helpful comments concerning our manuscript and for exciting discussions about the assignment process. We are also grateful to Dr. Dan Mullen for synthesizing NAVL.

Supporting Information Available: A table showing all the homonuclear and heteronuclear dipolar couplings used in the simulations (Figure 13) and additional information for Figures 4 and 5 that plot the PDSD cross-peak intensity divided by the diagonal peak intensity for NAL and NAVL, respectively. Also, additional information for Figures 10 and 12, which plot all cross-peak intensities for both the value of the ^1H spinlock and the percentage of MMHH for the PMPT experiment, is provided. This material is available free of charge via the Internet at http://pubs.acs.org.

References and Notes

(1) Naito, A. Structure Elucidation of Membrane-Associated Peptides and Proteins in Oriented Bilayers by Solid-State NMR Spectroscopy. *Solid State Nucl. Magn. Reson.* **2009**, *36*, 67–76.

(2) De Angelis, A. A.; Howell, S. C.; Nevzorov, A. A.; Opella, S. J. Structure Determination of a Membrane Protein with Two Trans-Membrane Helices in Aligned Phospholipid Bicelles by Solid-State NMR Spectroscopy. *J. Am. Chem. Soc.* **2006**, *128*, 12256–12267.

(3) Park, S. H.; Mrse, A. A.; Nevzorov, A. A.; Mesleh, M. F.; Oblatt-Montal, M.; Montal, M.; Opella, S. J.; Valentine, K. G.; Mesleh, M. F.; Opella, S. J.; Ikura, M.; Ames, J. B. Three-Dimensional Structure of the Channel-Forming Trans-Membrane Domain of Virus Protein "u" (Vpu) from HIV-1 Structure, Topology, and Dynamics of Myristoylated Recoverin Bound to Phospholipid Bilayers. *J. Mol. Biol.* **2003**, *333*, 409–424.

(4) Li, C.; Yi, M.; Hu, J.; Zhou, H. X.; Cross, T. A. Solid-State NMR and MD Simulations of the Antiviral Drug Amantadine Solubilized in DMPC Bilayers. *Biophys. J.* **2008**, *94*, 1295–1302.

(5) Durr, U. H.; Yamamoto, K.; Im, S. C.; Waskell, L.; Ramamoorthy, A. Solid-State NMR Reveals Structural and Dynamical Properties of a Membrane-Anchored Electron-Carrier Protein, Cytochrome b5. *J. Am. Chem. Soc.* **2007**, *129*, 6670–6671.

(6) Henzler Wildman, K. A.; Lee, D. K.; Ramamoorthy, A. Mechanism of Lipid Bilayer Disruption by the Human Antimicrobial Peptide, LL-37. *Biochemistry* **2003**, *42*, 6545–6558.

(7) Traaseth, N. J.; Shi, L.; Verardi, R.; Mullen, D.; Barany, G.; Veglia, G. Determination of Membrane Protein Structure and Topology using a Hybrid Solution and Solid-State NMR Approach. *Proc. Natl. Acad. Sci. U.S.A.* **2009**, *106*, 10165–10170.

(8) Traaseth, N. J.; Ha, K. N.; Verardi, R.; Shi, L.; Buffy, J. J.; Masterson, L. R.; Veglia, G. Structural and Dynamic Basis of Phospholamban and Sarcolipin Inhibition of Ca(2+)-ATPase. *Biochemistry* **2008**, *47*, 3–13.

(9) Buffy, J. J.; Traaseth, N. J.; Mascioni, A.; Gor'kov, P. L.; Chekmenev, E. Y.; Brey, W. W.; Veglia, G. Two-Dimensional Solid-State NMR Reveals Two Topologies of Sarcolipin in Oriented Lipid Bilayers. *Biochemistry* **2006**, *45*, 10939–10946.

(10) Fu, R.; Gordon, E. D.; Hibbard, D. J.; Cotten, M. High Resolution Heteronuclear Correlation NMR Spectroscopy of an Antimicrobial Peptide in Aligned Lipid Bilayers: Peptide-Water Interactions at the Water-Bilayer Interface. *J. Am. Chem. Soc.* **2009**, *131*, 10830–10831.

(11) Sau, S. P.; Ramanathan, K. V. Visualization of Enantiomers in the Liquid-Crystalline Phase of a Fragmented DNA Solution. *J. Phys. Chem. B* **2009**, *113*, 1530–1532.

(12) Wu, C. H.; Ramamoorthy, A.; Opella, S. J. High-Resolution Heteronuclear Dipolar Solid-State NMR Spectroscopy. *J. Magn. Reson.* **1994**, *109*, 270–272.

(13) Yamamoto, K.; Lee, D. K.; Ramamoorthy, A. Broadband-PISEMA Solid-State NMR Spectroscopy. *Chem. Phys. Lett.* **2005**, *407*, 289–293.

(14) Nevzorov, A. A.; Opella, S. J. Selective Averaging for High-Resolution Solid-State NMR Spectroscopy of Aligned Samples. *J. Magn. Reson.* **2007**, *185*, 59–70.

(15) Dvinskikh, S. V.; Yamamoto, K.; Ramamoorthy, A. Heteronuclear Isotropic Mixing Separated Local Field NMR Spectroscopy. *J. Chem. Phys.* **2006**, *125*, 34507.

(16) Gopinath, T.; Veglia, G. Sensitivity Enhancement in Static Solid-State NMR Experiments Via Single- and Multiple-Quantum Dipolar Coherences. *J. Am. Chem. Soc.* **2009**, *131*, 5754–5756.

(17) Gopinath, T.; Verardi, R.; Traaseth, N. J.; Veglia, G. Sensitivity Enhancement of Separated Local Field Experiments: Application to Membrane Proteins. *J. Phys. Chem. B* **2010**, *114*, 5089–5095.

(18) Gopinath, T.; Traaseth, N. J.; Mote, K.; Veglia, G. Sensitivity Enhanced Heteronuclear Correlation Spectroscopy in Multidimensional Solid-State NMR of Oriented Systems Via Chemical Shift Coherences. *J. Am. Chem. Soc.* **2010**, *132*, 5357–5363.

(19) Nevzorov, A. A.; Opella, S. J. Structural Fitting of PISEMA Spectra of Aligned Proteins. *J. Magn. Reson.* **2003**, *160*, 33–39.

(20) Bertram, R.; Asbury, T.; Fabiola, F.; Quine, J. R.; Cross, T. A.; Chapman, M. S. Atomic Refinement with Correlated Solid-State NMR Restraints. *J. Magn. Reson.* **2003**, *163*, 300–309.

(21) Shi, L.; Traaseth, N. J.; Verardi, R.; Cembran, A.; Gao, J.; Veglia, G. A Refinement Protocol to Determine the Structure, Topology, and Depth of Insertion of Membrane Proteins using Hybrid Solution and Solid-State Restraints. *J. Biomol. NMR* **2009**, *44*, 195–205.

(22) Marassi, F. M.; Opella, S. J. A Solid-State NMR Index of Helical Membrane Protein Structure and Topology. *J. Magn. Reson.* **2000**, *144*, 150–155.

(23) Wang, J.; Denny, J.; Tian, C.; Kim, S.; Mo, Y.; Kovacs, F.; Song, Z.; Nishimura, K.; Gan, Z.; Fu, R.; Quine, J. R.; Cross, T. A. Imaging Membrane Protein Helical Wheels. *J. Magn. Reson.* **2000**, *144*, 162–167.

(24) Mesleh, M. F.; Lee, S.; Veglia, G.; Thiriot, D. S.; Marassi, F. M.; Opella, S. J. Dipolar Waves Map the Structure and Topology of Helices in Membrane Proteins. *J. Am. Chem. Soc.* **2003**, *125*, 8928–8935.

(25) Mascioni, A.; Veglia, G. Theoretical Analysis of Residual Dipolar Coupling Patterns in Regular Secondary Structures of Proteins. *J. Am. Chem. Soc.* **2003**, *125*, 12520–12526.

(26) Page, R. C.; Kim, S.; Cross, T. A. Transmembrane Helix Uniformity Examined by Spectral Mapping of Torsion Angles. *Structure* **2008**, *16*, 787–797.

(27) Vosegaard, T.; Nielsen, N. C. Towards High-Resolution Solid-State NMR on Large Uniformly 15N- and [13C,15N]-Labeled Membrane Proteins in Oriented Lipid Bilayers. *J. Biomol. NMR* **2002**, *22*, 225–247.

(28) Igumenova, T. I.; Wand, A. J.; McDermott, A. E. Assignment of the Backbone Resonances for Microcrystalline Ubiquitin. *J. Am. Chem. Soc.* **2004**, *126*, 5323–5331.

(29) Reif, B.; Hohwy, M.; Jaroniec, C. P.; Rienstra, C. M.; Griffin, R. G. NH-NH Vector Correlation in Peptides by Solid-State NMR. *J. Magn. Reson.* **2000**, *145*, 132–141.

(30) Quine, J. R.; Achuthan, S.; Asbury, T.; Bertram, R.; Chapman, M. S.; Hu, J.; Cross, T. A. Intensity and Mosaic Spread Analysis from PISEMA Tensors in Solid-State NMR. *J. Magn. Reson.* **2006**, *179*, 190–198.

(31) Traaseth, N. J.; Buffy, J. J.; Zamoon, J.; Veglia, G. Structural Dynamics and Topology of Phospholamban in Oriented Lipid Bilayers using Multidimensional Solid-State NMR. *Biochemistry* **2006**, *45*, 13827–13834.

(32) Traaseth, N. J.; Verardi, R.; Torgersen, K. D.; Karim, C. B.; Thomas, D. D.; Veglia, G. Spectroscopic Validation of the Pentameric Structure of Phospholamban. *Proc. Natl. Acad. Sci. U.S.A.* **2007**, *104*, 14676–14681.

(33) Muller, S. D.; De Angelis, A. A.; Walther, T. H.; Grage, S. L.; Lange, C.; Opella, S. J.; Ulrich, A. S. Structural Characterization of the Pore Forming Protein TatAd of the Twin-Arginine Translocase in Membranes by Solid-State 15N-NMR. *Biochim. Biophys. Acta* **2007**, *1768*, 3071–3079.

(34) De Angelis, A. A.; Nevzorov, A. A.; Park, S. H.; Howell, S. C.; Mrse, A. A.; Opella, S. J. High-Resolution NMR Spectroscopy of Membrane Proteins in Aligned Bicelles. *J. Am. Chem. Soc.* **2004**, *126*, 15340–15341.

(35) Szeverenyi, N. M.; Sullivan, M. J.; Maciel, G. E. Observation of Spin Exchange by Two-Dimensional Fourier Transform 13C Cross Polarization-Magic-Angle Spinning. *J. Magn. Reson.* **1982**, *47*, 462–475.

(36) Suter, D.; Ernst, R. R. Spin Diffusion in Resolved Solid-State NMR Spectra. *Phys. Rev. B* **1985**, *32*, 5608–5627.

(37) Xu, J.; Struppe, J.; Ramamoorthy, A. Two-Dimensional Homonuclear Chemical Shift Correlation Established by the Cross-Relaxation Driven Spin Diffusion in Solids. *J. Chem. Phys.* **2008**, *128*, 052308.

(38) Nevzorov, A. A. Mismatched Hartmann-Hahn Conditions Cause Proton-Mediated Intermolecular Magnetization Transfer between Dilute Low-Spin Nuclei in NMR of Static Solids. *J. Am. Chem. Soc.* **2008**, *130*, 11282–11283.

(39) Cross, T. A.; Frey, M. H.; Opella, S. J. Nitrogen-15 Spin Exchange in a Protein. *J. Am. Chem. Soc.* **1983**, *105*, 7471–7473.

(40) Marassi, F. M.; Gesell, J. J.; Valente, A. P.; Kim, Y.; Oblatt-Montal, M.; Montal, M.; Opella, S. J. Dilute Spin-Exchange Assignment of Solid-State NMR Spectra of Oriented Proteins: Acetylcholine M2 in Bilayers. *J. Biomol. NMR* **1999**, *14*, 141–148.

(41) Lewandowski, J. R.; De Paepe, G.; Griffin, R. G. Proton Assisted Insensitive Nuclei Cross Polarization. *J. Am. Chem. Soc.* **2007**, *129*, 728–729.

(42) De Paepe, G.; Lewandowski, J. R.; Loquet, A.; Bockmann, A.; Griffin, R. G. Proton Assisted Recoupling and Protein Structure Determination. *J. Chem. Phys.* **2008**, *129*, 245101.

(43) Lewandowski, J. R.; De Paepe, G.; Eddy, M. T.; Griffin, R. G. (15)N-(15)N Proton Assisted Recoupling in Magic Angle Spinning NMR. *J. Am. Chem. Soc.* **2009**, *131*, 5769–5776.

(44) Knox, R. W.; Lu, G. J.; Opella, S. J.; Nevzorov, A. A. A Resonance Assignment Method for Oriented-Sample Solid-State NMR of Proteins. *J. Am. Chem. Soc.* **2010**, *132*, 8255–8257.

(45) Carroll, P. J.; Stewart, P. L.; Opella, S. J. Structures of Two Model Peptides: N-Acetyl-D, L-Valine and N-Acetyl-L-Valyl-L-Leucine. *Acta Crystallogr., Sect. C* **1990**, *46*, 243–246.

(46) Gor'kov, P. L.; Chekmenev, E. Y.; Li, C.; Cotten, M.; Buffy, J. J.; Traaseth, N. J.; Veglia, G.; Brey, W. W. Using Low-E Resonators to Reduce RF Heating in Biological Samples for Static Solid-State NMR Up to 900 MHz. *J. Magn. Reson.* **2007**, *185*, 77–93.

(47) Robyr, P.; Meier, B. H.; Ernst, R. R. Radio-Frequency-Driven Nuclear Spin Diffusion in Solids. *Chem. Phys. Lett.* **1989**, *162*, 417–423.

(48) Robyr, P.; Gan, Z. Radiofrequency-Driven and Slow-Magic-Angle-Sample-Spinning Polarization-Transfer Techniques: A Comparative Study. *J. Magn. Reson.* **1998**, *131*, 254–260.

(49) Nevzorov, A. A. High-Resolution Local Field Spectroscopy with Internuclear Correlations. *J. Magn. Reson.* **2009**, *201*, 111–114.

(50) Lange, A.; Luca, S.; Baldus, M. Structural Constraints from Proton-Mediated Rare-Spin Correlation Spectroscopy in Rotating Solids. *J. Am. Chem. Soc.* **2002**, *124*, 9704–9705.

(51) Ramamoorthy, A.; Gierasch, L. M.; Opella, S. J. Three-Dimensional Solid-State NMR Correlation Experiment with 1H Homonuclear Spin Exchange. *J. Magn. Reson., Ser. B* **1996**, *111*, 81–84.

(52) Bronniman, C. E.; Szeverenyi, N. M.; Maciel, G. E. 13C Spin Diffusion of Adamantane. *J. Chem. Phys.* **1983**, *79*, 3694–3700.

(53) deAzevedo, E. R.; Bonagamba, T. J.; Schmidt-Rohr, K. Pure-Exchange Solid-State NMR. *J. Magn. Reson.* **2000**, *142*, 86–96.

(54) Vosegaard, T.; Nielsen, N. C. Improved Pulse Sequences for Pure Exchange Solid-State NMR Spectroscopy. *Magn. Reson. Chem.* **2004**, *42*, 285–290.

(55) Hartmann, S. R.; Hahn, E. L. *Phys. Rev.* **1962**, *128*, 2042–2053.

(56) Wu, C. H.; Ramamoorthy, A.; Gierasch, L. M.; Opella, S. J. Simultaneous Characterization of the Amide 1H Chemical Shift, 1H-15N Dipolar, and 15N Chemical Shift Interaction Tensors in a Peptide Bond by Three-Dimensional Solid-State NMR Spectroscopy. *J. Am. Chem. Soc.* **1995**, *117*, 6148–6149.

(57) Stringer, J. A.; Bronnimann, C. E.; Mullen, C. G.; Zhou, D. H.; Stellfox, S. A.; Li, Y.; Williams, E. H.; Rienstra, C. M. Reduction of RF-Induced Sample Heating with a Scroll Coil Resonator Structure for Solid-State NMR Probes. *J. Magn. Reson.* **2005**, *173*, 40–48.

(58) Ishii, Y.; Tycko, R. Multidimensional Heteronuclear Correlation Spectroscopy of a Uniformly ^{15}N- and ^{13}C-Labeled Peptide Crystal: Toward Spectral Resolution, Assignment, and Structure Determination of Oriented Molecules in Solid-State NMR. *J. Am. Chem. Soc.* **2000**, *122*, 1443–1455.

JP105718R